



HAL
open science

RPV fracture toughness of various metallurgical zones at very high fluences

B. Tanguy, B. Marini, P. Wident, P. Todeschini, P. Joly

► **To cite this version:**

B. Tanguy, B. Marini, P. Wident, P. Todeschini, P. Joly. RPV fracture toughness of various metallurgical zones at very high fluences. FONTEVRAUD 9, Sep 2018, Avignon, France. cea-02338573

HAL Id: cea-02338573

<https://cea.hal.science/cea-02338573>

Submitted on 24 Feb 2020

HAL is a multi-disciplinary open access archive for the deposit and dissemination of scientific research documents, whether they are published or not. The documents may come from teaching and research institutions in France or abroad, or from public or private research centers.

L'archive ouverte pluridisciplinaire **HAL**, est destinée au dépôt et à la diffusion de documents scientifiques de niveau recherche, publiés ou non, émanant des établissements d'enseignement et de recherche français ou étrangers, des laboratoires publics ou privés.

RPV fracture toughness of various metallurgical zones at very high fluences

B. Tanguy¹, B. Marini², P. Wident², P. Todeschini³, P. Joly⁴

¹ CEA Saclay, Université Paris-Saclay, DEN, Service d'Etudes des Matériaux Irradiés, 91191 Gif-sur-Yvette, France

² CEA Saclay, Université Paris-Saclay, DEN, Service d'Etudes de Métallurgie Appliquée, 91191 Gif-sur-Yvette, France

³ EDF Lab Les Renardières, Materials and Mechanics of Components Department, F-77818 Moret-sur-Loing, France

⁴FRAMATOME, Technical Direction and Engineering, Mechanical Engineering Division,, 92084 Paris La Défense, France

*Main Author, E-mail: benoit.tanguy@cea.fr

Keywords: *RPV steel, Fracture toughness, base metal, weld, underclad HAZ, Irradiation, high fluences*

Abstract

The monitoring and assessment of aging effects of reactor pressure vessels (RPV) of PWRs during operation life is performed by means of an irradiation surveillance program. In the surveillance program of the PWRs of the French fleet, a large database of Charpy transition shifts and fracture toughness has been established up to neutron fluence values corresponding to 40 years of operation and over, for the base metals, welds and Heat Affected Zones (HAZ) of the core zone. Much fewer fracture toughness data are nevertheless available for relevant materials at higher fluence values, especially for underclad heat affected zones (UHAZ) that are not monitored by the irradiation surveillance program. This paper presents the R&D program carried out by CEA, EDF and FRAMATOME in order to provide fracture toughness data to complement the irradiation surveillance program in a higher fluence range and including samples of underclad heat affected zones. The irradiation exposure of this program was performed in OSIRIS reactor at CEA Saclay up to a maximum fluence level of $14 \cdot 10^{19}$ n/cm² ($E > 1$ MeV). Fracture toughness properties were characterized for two base metals, a fine grain a coarse grain HAZ and a weld metal with Pre-cracked Charpy V (PCCV) specimens. The fracture toughness data were analyzed with the Master Curve methodology and compared to the RCC-M lower bound curve.

Introduction

The monitoring and assessment of aging effects in reactor pressure vessels (RPV) during service is performed by means of irradiation surveillance programs. Base metal from forged shells in 16MND5 grade steel, their circumferential weld and heat affected zone (HAZ) as well as a reference material from a heavy section hot rolled plate in 18MND5 grade are those monitored in the French surveillance program [Brillaud1992]. Changes in mechanical properties are assessed through tensile and Charpy V-Notch specimens where only Charpy transition temperature shift is used to characterize the embrittlement. In conjunction with the surveillance data, embrittlement trend curves (ETCs) are used to predict the irradiation induced change in fracture toughness needed for RPV integrity assessments [Todeschini2010]. Fracture toughness lower bound curve $K_{1c}(T-RT_{NDT})$ and its shift based on the predictions of the ETCs are compared to fracture toughness measurements at different neutron fluence levels based on the fracture toughness specimens located in the surveillance capsules. For the French surveillance irradiation program, a large database has been established up to fluences corresponding to more than 40 years of operation for the RPV. Fewer fracture toughness data are available for relevant materials at higher fluences. These data, which can only be obtained in Materials Testing Reactors (MTR), were identified as important in order to check the validity domain of the toughness prediction method. Moreover, underclad heat affected zones (UHAZ) are not monitored by the irradiation surveillance program, although they may contain specific microstructures due to the cladding process and conditions [Todeschini2014]. This paper presents the R&D program carried out by CEA, EDF and FRAMATOME to provide fracture toughness data to complement the irradiation surveillance program in the relevant fluence range and including underclad heat affected zones. The materials and irradiation conditions are described in the first section. Mechanical testing is then detailed. The third section presents the tensile and fracture toughness properties for the five types of microstructure investigated. The

fracture toughness data are analyzed with Master Curve methodology and compared to the ETC prediction. The last section is dedicated to fractographic investigations.

Materials and Irradiation conditions

The two base metals (BM1 and BM2) used in this study are 16MND5 (similar to A508 Cl3) steels taken from forged nozzle shell cut-outs of two pressurized water reactors (PWR). The weld metal (WM1) comes from a RPV weld mockup representative of the weld between core shells. The welding was done by submerged arc with AS89 flux. Chemical compositions of BM and WM materials are given in Table 1. Underclad heat affected zone (UHAZ) was elaborated by cladding a mockup on BM1 base metal. Before cladding, the inner surface of the nozzle shell cut-out (disk of diameter 1240 mm and thickness 230 mm) was machined in order to obtain a flat surface. Cladding was obtained by submerged arc welding (SAW) with two layers of austenitic steels, 309L for the first layer and 308L for the second layer. Preheating at 150°C-200°C was applied before deposition of the first layer in order to limit the possibility of cold cracking beneath the cladding. After cladding, two Post Weld heat treatments at 550°C and 610°C were applied¹. These heat treatments aim to simulate intermediate as well as final post weld heat treatment (PWHT) applied to the RPV during the manufacturing process. The metallurgical structure and properties of the HAZ are controlled by the thermal cycles and the weld bead deposit sequence. Due to the high heat input of the strip cladding process a layer of underlying base material is heated to a high temperature which generates a coarse grain austenitic microstructure near the fusion line (noted A on Figure1). The deposition of the second layer produces reheating of the underlying base material to an intermediate temperature. This heating results in a new austenite transformation of the underlying base material, and a new fine grain microstructure (zone B on Figure 1). In this study, coarse grain heat affected zone remains in the first layer HAZ resulting from the absence of overlapping of the second layer HAZs. Micrographic investigations were performed from fusion line to base metal and confirm a coarse grain zone with grain size from ~250 µm near the interface to ~10 µm at 9 mm from the interface (see Figure 1a.zoner A). In zone B of Figure 1a (HAZ of layer 2), the grain size varies from 50 µm near the fusion line to ~8 µm at 5 mm from the interface.

REF	C	S	P	Mn	Si	Ni	Cr	Mo	V	Cu	Co
BM1	0.16	0.008	0.009	1.32	0.22	0.72	0.16	0.51	0.006	0.06	0.01
BM2	0.18	0.007	0.011	1.31	0.24	0.70	0.18	0.51	0.006	0.08	0.02
WM1	0.07	0.008	0.008	1.59	0.422	0.76	0.164	0.586	/	0.048	/

Table 1: Chemical composition of materials (%wt) used in this study (BM: base metal, WM: weld metal)

In order to characterize the fracture toughness of coarse grain and fine grains HAZ, the precracking fronts of PCCV specimens were located precisely in the HAZ based on polishing and Nital etching of side surfaces of each specimen. Fatigue pre-crack fronts are located between 0.5 and 1 mm from fusion line in first layer HAZ, corresponding to a grain size of about 150 µm, and at 3 mm from fusion line in second layer HAZ corresponding to a grain size of about 10 µm. Example of specimen positioning is given in Figure 1b and Figure 1c, for fine grain (FG) HAZ and coarse grain (CG) HAZ, respectively.

The sampling of the specimens was done in the frame of a larger project including a thermal ageing program. To minimize unirradiated state issues, the batches of specimens to characterize a given metallurgical zone in its various states were formed by random selection in the whole set of specimens. A potential side effect of this large scale sampling is an increase of the data scatter because of the non-negligible distances between specimen positions within a given batch.

Specimens were irradiated in the Materials Testing Reactor Osiris (CEA Saclay, France) under mixed spectrum up to a maximal fast neutron fluence of $\sim 14.2 \cdot 10^{19} \text{ n.cm}^{-2}$ ($E > 1\text{MeV}$) at a temperature of 288°C (+5/-7 °C) with a flux of $4.5 \cdot 10^{12} \text{ n.cm}^{-2}.\text{s}^{-1}$ (see Table 2). The maximum Iron damage is about 0.2 dpa. Due to axial flux gradient in the reactor, fluence and temperature variations are observed between the specimens depending on their locations in the irradiation rig. Mean fluence and mean temperature for each metallurgical zone for fracture toughness specimens are reported in Table 2. It is underlined that the tensile specimens were located close to the fracture toughness specimens in the irradiation rig

¹ First heat treatment: heating at 40°C/h, hold 12h15, cooling rate 40°C/h up to 80°C. Second heat treatment: heating at 50°C/h, hold 6h15, cooling rate 30°C/h up to 80°C.

so that the irradiation conditions are very close for both geometries.

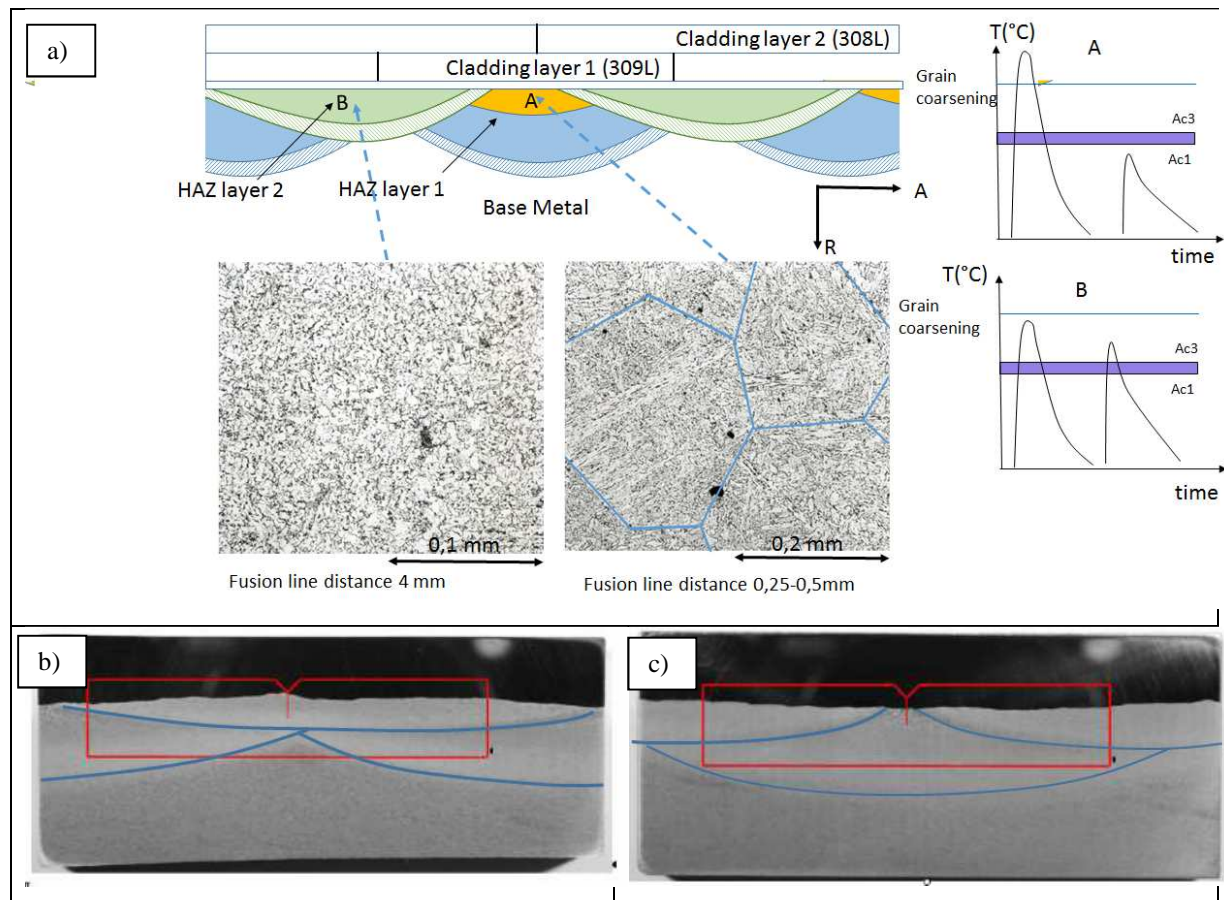


Figure 1: Cladding HAZ for toughness characterization. a) Metallurgical structures of the first and second layer HAZ. b) Precracked Charpy specimen positioning in the fine grain second layer HAZ, c) Precracked Charpy specimen positioning in the coarse grain first layer HAZ. The metallurgical directions are referred to as: L, A and R for the longitudinal (tangential direction in a shell), axial and radial directions, respectively.

Metallurgical zone	BM1	BM2	WM1	CG HAZ	FG HAZ
Mean fluence ϕ (n.cm ⁻²)	13.2 10 ¹⁹	14.1 10 ¹⁹	14.05 10 ¹⁹	12.44 10 ¹⁹	11.6 10 ¹⁹
Mean temperature (°C)	285.2	288.2	282	288	286.3

Table 2: Irradiation conditions for the RPV metallurgical zones performed in the Material Testing reactor Osiris

Mechanical testing

Fracture toughness properties have been measured through pre-cracked Charpy-V (PCCV) specimen. This geometry was chosen considering the geometrical constraints to study the underclad HAZ fracture toughness. The use of the Charpy size specimen for fracture toughness testing was largely investigated in literature and it is nowadays accepted that such a geometry can provide a reliable transition temperature, T₀, if the number of specimens is large enough. As compared to the Compact Tension geometry, a bias of 10 to 15°C (a lower T₀ being obtained with Charpy-size specimens) is usually reported in literature (see e.g. [Joyce 2001, Joye2005, Lucon2003]) and is due to the difference of constraint between the two geometries. BM and WM specimens were machined in A-L orientations (Loading along axial direction and propagation through circumferential direction). HAZ specimens were machined in A-R orientations as shown in Figure 1 so that the crack propagates through the HAZ microstructure towards the base metal (radial propagation). The fracture toughness K_{Jc} was evaluated according to ISO-12135 standard [ISO12135]. The length of fatigue precrack was measured from the fracture surface

after the fracture toughness test and validity was evaluated with regards to K_{Jc} value, fatigue crack length and slow-stable crack growth extent. The Master Curve methodology has been applied following standard ASTM E1921 [ASTME1921] to determine the reference temperature T_0 and the tolerance bounds 2%, 50% and 98% of the Master Curve for a thickness of 1T (25.4 mm). For the irradiated state, 12 specimens were tested per metallurgical zone whereas between 12 and 19 specimens were tested at the un-irradiated state. The standard deviation on the estimate of T_0 has been evaluated to $\sim 6^\circ\text{C}$ by $\sigma = \frac{\beta}{\sqrt{r}} (^\circ\text{C})$ where r is the total number of valid specimens used to establish the value of T_0 and β is a parameter given in appendix X4 of ASTM E1921. Conventional tensile properties were determined in order to evaluate the maximum K_{Jc} capacity of the pre-cracked Charpy specimen following ASTM E1921 [ASTME1921] ($K_{Jc}(\text{limit}) = [Eb_0\sigma_y / \{30(1 - \nu^2)\}]^{1/2}$). They have been measured through tensile tests on flat tensile (FT) specimens with their gauge length parallel to axial orientation for BM, WM and FG HAZ², at a mean strain rate of 5.10^{-4}s^{-1} [ISO6892]. Testing temperatures were between -100°C and $+100^\circ\text{C}$ for BM and WM whereas it was between -50°C and RT for HAZ at the irradiated state (-150°C and RT at the un-irradiated state). Due to the limited number of specimens in the irradiation rig only one specimen was tested at each temperature at the irradiated state. Mechanical characterizations has been performed at CEA Saclay, in LECl hot cells for irradiated materials.

Results

The evolution of the yield stress (as defined by $R_{p0.2\%}$) as a function of test temperature is given on Figure 2 at the un-irradiated state (left) and irradiated state (right). At the un-irradiated state, tensile properties of BM1 and BM2 are close whereas WM1 and FG HAZ show higher yield stress. A significant irradiation hardening is observed after irradiation for all the metallurgical zones considered as shown on figure 2 (right). Adjustments of experimental data have been done using the relation $R_{p0.2}(T) = A + B \exp(-C(T + 273.15))$ (where A , B and C are material parameters) and are shown on both graphs of Figure 2. Evolutions of $R_{p0.2}(T)$ have been used to determine $K_{Jc}(\text{limit})$ as a function of temperature and fluence.

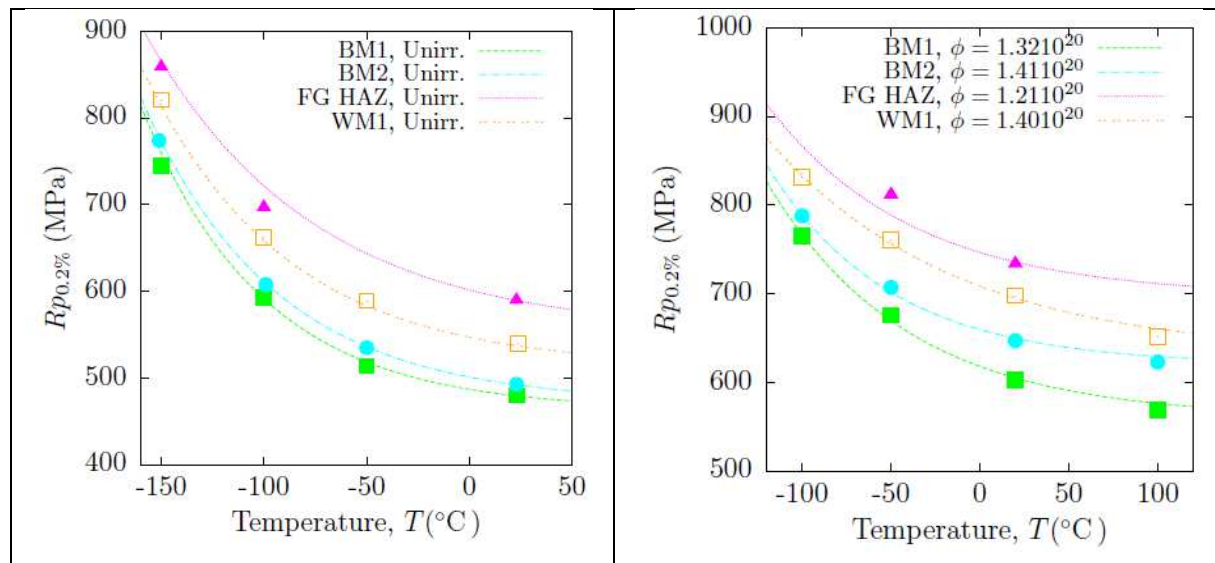


Figure 2: Yield stress ($R_{p0.2}$) evolution with temperature for base metals (BM1 and BM2), weld metal (WM1) and fine grain HAZ.

Fracture toughness results for BM, HAZ and WM are given on figures 3, 4 and 6, respectively. For the irradiated state, the experimental data reported on these figures are the raw data obtained without any correction to take into account variations of fluence or of irradiation temperature between specimens or between metallurgical zones as reported in table 2. T_0 values are reported in each figure.

On these figures, the lower bound toughness curve has been added for each material. The lower

² Tensile specimens were not sampled in CG HAZ due to its small size. For WM, tensile specimens are perpendicular to the weld axis.

bound toughness curve, $K_{Ic}(T)$ is given by [RCC-M 2007]:

$$K_{Ic}(T) = 40 + 0.09(T - RT_{NDT}) + 20 * \exp[0.038 * (T - RT_{NDT})] \quad (1)$$

In this equation, the parameter RT_{NDT} and its evolution with fluence has been determined by the irradiation embrittlement correlation used for EDF RPV fleet [Todeschini2010]:

$$RT_{NDT}(\phi) = RT_{NDT}(0) + \Delta RT_{NDT}(\phi) + \text{Margin} \quad (2)$$

$$\text{Where } \Delta RT_{NDT}(\phi) = A[1 + 35.7(P - 0.008)_+ + 6.6(Cu - 0.08)_+ + 5.8Ni^2Cu][\phi / 10^{19}]^{0.59} \quad (3)$$

A is a scale factor equal to 15.4 and 15.8 for base metal (forgings) and weld metal, respectively. Margin is taken as two times the standard deviation, i.e. 20.8°C and 26.6°C for base metal and weld metal, respectively.

For both base metals, a large scatter is observed at the un-irradiated state as shown on Figure 3a, where few fracture toughness results are below the 2% fractile (dotted lines) of the master curve. Similar trends are observed after irradiation (Figure 3b) with few fracture toughness results below the 2% fractile only for the BM1. It is noted that for the two base metals considered the lower bound character of the RCC-M curve is verified for a level of fluence up to $\sim 14 \cdot 10^{19} \text{ n/cm}^2$ ($E > 1\text{MeV}$) and that a significant conservatism is obtained in the transition region for this level of fluence. A direct comparison of the two base metals for the same fluence level, ϕ_{ref} , of $13.7 \cdot 10^{19} \text{ n/cm}^2$ ($E > 1\text{MeV}$) is given on figure 5a. In this figure, a corrected test temperature is considered for each test in order to take into account the fluence variation and the irradiation temperature variation for each specimen. The corrected temperature is based on the equation (3) for fluence and on the embrittlement temperature correction proposed in [Todeschini, 2010]:

$\Delta RT_{NDT}(\text{°C}) = \Delta RT_{NDT}(288\text{°C}) [1 - 0.0153(T - 288)]$; so that $T_{corrected} = T_{test} + (\Delta RT_{NDT}(288\text{°C})(\phi_{ref}) - \Delta RT_{NDT}(T_{irr})(\phi_{irr}))$ where T_{irr} et ϕ_{irr} , are the irradiation temperature and fluence for each specimen. The reference temperature is then reevaluated based on the corrected temperatures. The comparison at the same fluence level of $13.7 \cdot 10^{19} \text{ n/cm}^2$ ($E > 1\text{MeV}$) with normalized temperatures confirms that the RCC-M curve bounds the data and that BM1 has a higher T_0 than BM2.

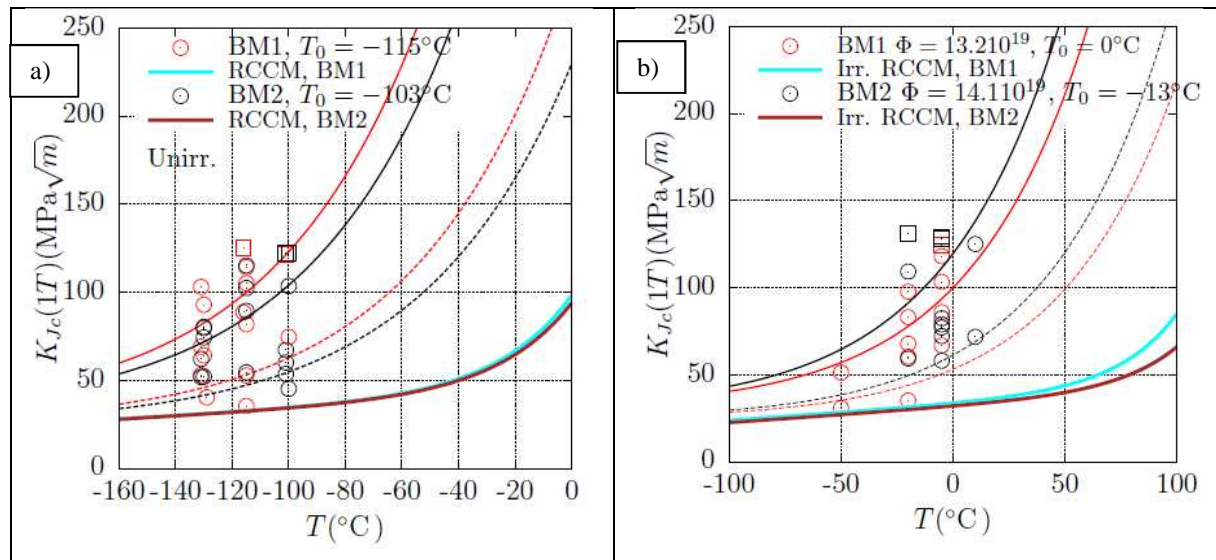


Figure 3: Fracture toughness (IT) for base metals (BM1 and BM2) as a function of temperature. a: Un-irradiated state, b: Irradiated. Full and dotted lines represent the 50% and 2% fractile of master-curve, respectively. Square symbols correspond to censored data with $K_{Ic} > K_{Ic}(\text{limit})$. Initial RT_{NDT} values are -27°C and -25°C for BM1 and BM2, respectively.

Figure 4 shows the fracture toughness of FG and CG HAZ. The T_0 values at the un-irradiated state (-105°C and -127°C for CG and FG HAZ, respectively) are close to the T_0 of the BM1 metal (-115°C), the fine grain HAZ showing the highest fracture toughness (lowest T_0) and the coarse grain HAZ the lowest fracture toughness (the highest T_0). As shown on Figure 4a where the data for the BM1 are also reported, a similar large scatter of fracture toughness is also observed for CG and FG HAZ with few fracture toughness results below the 2% fractile for CG HAZ. Similar trends are observed after irradiation

(Figure 4b). Direct comparison of the CG HAZ, FG HAZ and BM1 for a fluence level, ϕ_{ref} , of $12.4 \cdot 10^{19} \text{ n/cm}^2$ ($E > 1\text{MeV}$) is given on figure 5b where normalization has been done as previously described. For this level of fluence, the fine grain HAZ has the highest fracture toughness (lowest T_0) and the coarse grain HAZ shows similar fracture toughness than the base metal ($T_0 = -7^\circ\text{C}$ and -6°C). The lower bound character of the RCCM curve for base metal is verified for both CG and FG HAZ for a level of fluence up to $\sim 12.4 \cdot 10^{19} \text{ n/cm}^2$ ($E > 1\text{MeV}$) as well as a significant conservatism in the transition region.

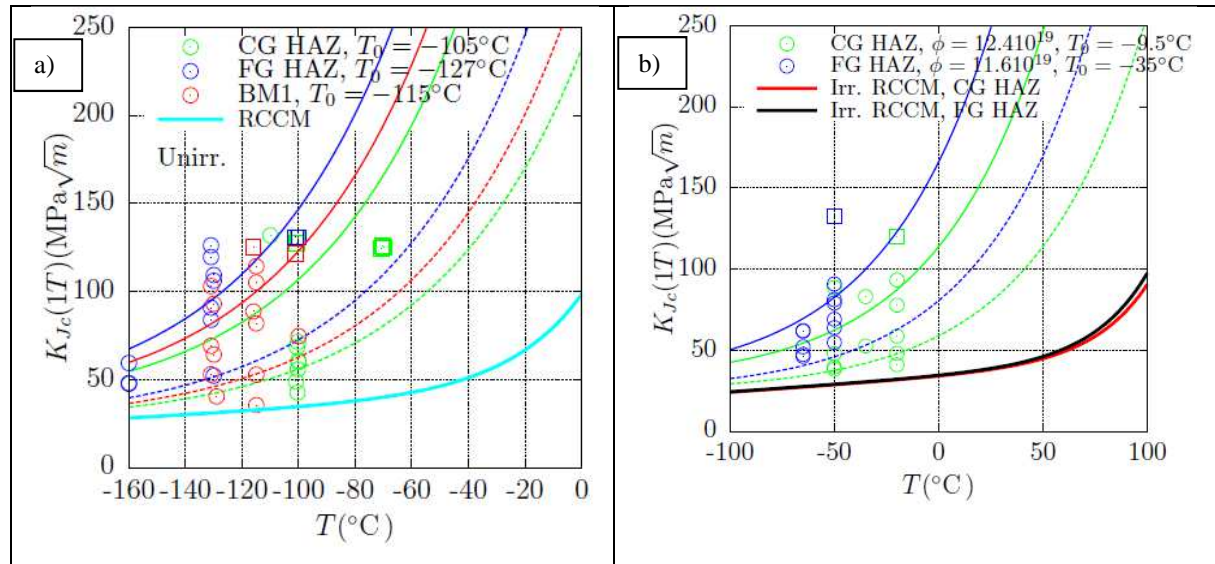


Figure 4: Fracture toughness (1T) for UHAZ (CH HAZ and FG HAZ) as a function of temperature. a: Unirradiated state, b: irradiated. Solid and dotted lines represent the 50% and 2% fractile of master-curve, respectively. Square symbols correspond to censored data with $K_{Jc} > K_{Jc}(\text{limit})$.

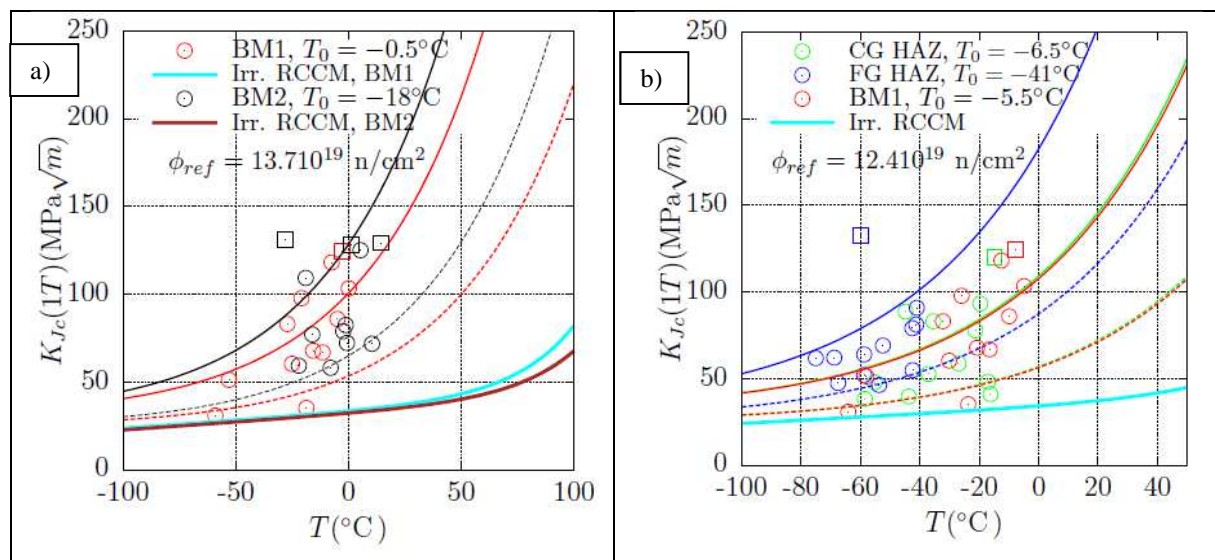


Figure 5: Comparison of fracture toughness (1T) after fluence and temperature normalization. a: Base metal at $13.7 \cdot 10^{19} \text{ n/cm}^2$, b: CH HAZ and FG HAZ and base metal at $12.4 \cdot 10^{19} \text{ n/cm}^2$. Solid and dotted lines represent the 50% and 2% fractile of master-curve, respectively. Square symbols correspond to censored data with $K_{Jc} > K_{Jc}(\text{limit})$.

The fracture toughness for the weld metal WM1 is shown on figure 6. At the un-irradiated state (Figure 6a), this metallurgical zone shows the highest T_0 (lowest fracture toughness) value amongst all the metallurgical zones characterized in this study. Interestingly, this microstructure shows less scatter than BM and HAZ and appears to be well described by the master curve fractile 2% and 50%. Again the lower bound character of the RCCM curve is confirmed both at un-irradiated state and for a fluence level

of $14 \cdot 10^{19} \text{ n/cm}^2$.

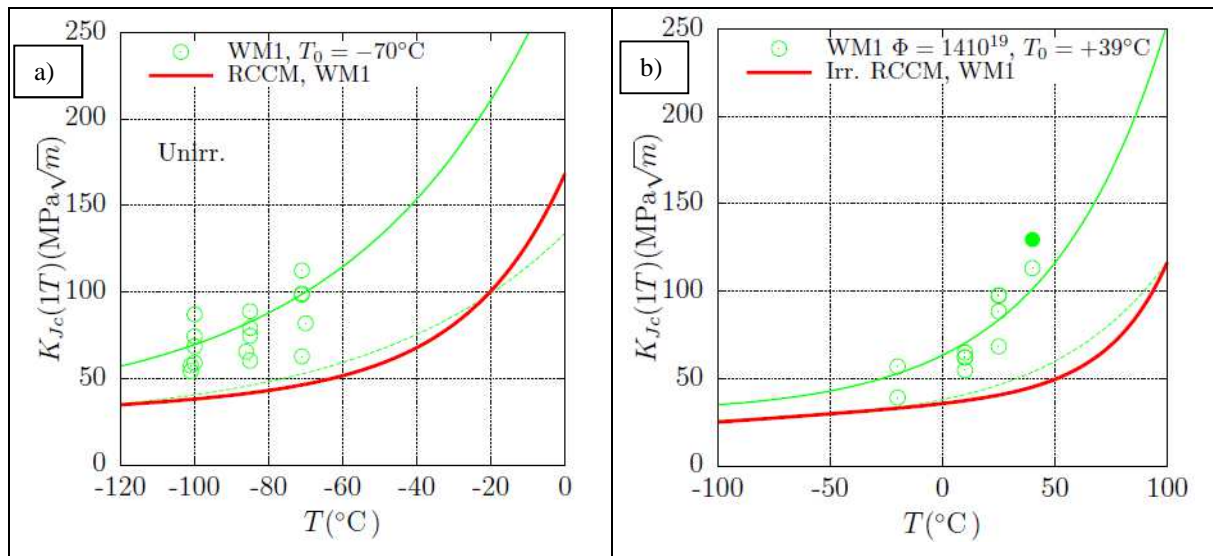


Figure 6: Fracture toughness (1T) for WM1 as a function of temperature. Left: Unirradiated state, Right: irradiated. Solid and dotted lines represent the 50% and 2% fractile of master-curve, respectively. Solid symbols correspond to censored data with $K_{Jc} > K_{Jc}(\text{limit})$. Initial RT_{NDT} value is -48°C

Fractographic investigations

Fractographic investigations were carried out for the different metallurgical zones to investigate the damage process associated to brittle fracture. For each investigated specimen, initiation site was identified by following a network of radiating major tear and river lines [Bouchet2005]. Considering the large scatter of K_{Jc} observed both for BM and U-HAZ, a particular attention was paid on the specimens showing low values of fracture toughness. Brittle fracture mode of RPV base metal at the un-irradiated state has been extensively characterized (see e.g. [Tanguy,2005]) and corresponds to transgranular cleavage fracture although materials with high level of chemical impurities (as phosphorous) can show localized inter-granular brittle fracture at the un-irradiated state as reported in [Chapuliot2010]. Figure 7 shows the initiation sites for two irradiated BM1 specimens with fracture toughness levels of $31 \text{ MPa}\cdot\text{m}^{0.5}$ and $83 \text{ MPa}\cdot\text{m}^{0.5}$ tested at -50°C and -20°C , respectively. The first specimen corresponds to a point below the 2% fractile on Figure 3b whereas the second specimen correspond to a point close to 50% fractile. For both specimens, cleavage fracture is the main mode of brittle fracture. For the specimen with the lowest fracture toughness, the initiation site is the closest to the fatigue crack front which is consistent with the lowest value of fracture toughness. It is noted that a small facet of intergranular decohesion is inferred to be at the immediate vicinity of the initiation site as indicated by a blue arrow on figure7b. However such facet can also be observed at the un-irradiated state so that no noticeable modification of brittle fracture mode was observed between un-irradiated and irradiated state for BM1 at this level of

fluence of $13.2 \cdot 10^{19} \text{ n.cm}^{-2}$.

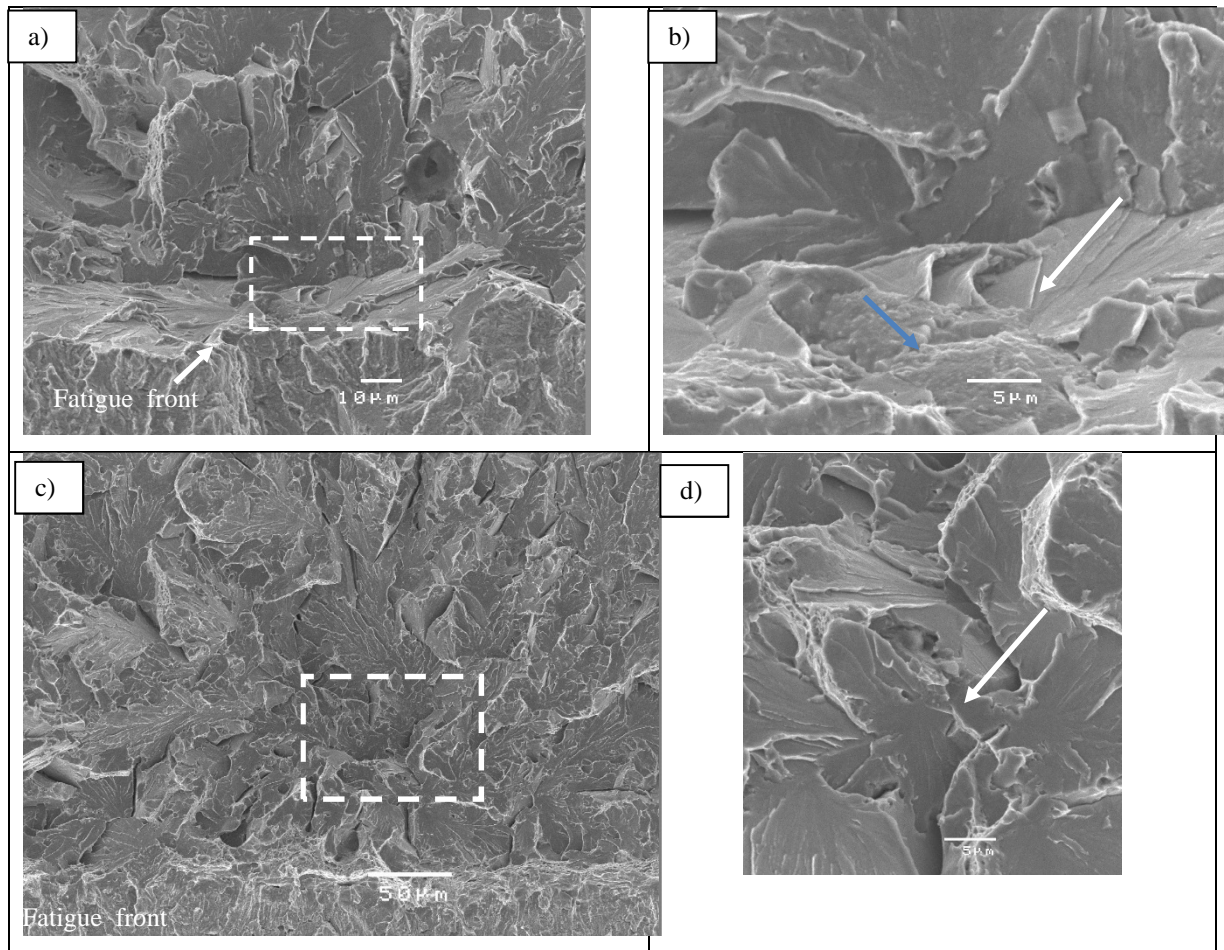


Figure 7: Fractographic investigations of BM1 at the irradiated state. a) and b): $KJc(1T) = 31 \text{ MPa.m}^{0.5}$ at -50°C , c) and d): $KJc(1T) = 83 \text{ MPa.m}^{0.5}$ at -20°C . White arrows indicate the initiation site of cleavage fracture. Blue arrow on b) indicates a decohesion facet.

Figure 8 and Figure 9 illustrate the fracture mode at the un-irradiated and irradiated state for two CG HAZ specimens with fracture toughness lower than $50 \text{ MPa.m}^{0.5}$. The fusion line is reported on these figures for each specimens. At the un-irradiated state, Figure 8 evidences that intergranular fracture areas can be located in the brittle fracture area where a mixed mode of fracture is observed: transgranular cleavage fracture and intergranular fracture. For this specimen, the cleavage fracture was initiated on a large area of intergranular fracture located in the close neighborhood of the fatigue crack front. Similar features have been observed at the irradiated state as shown in Figure 9. This type of fracture has been already observed after irradiation in simulated CGHAZ [Marini, 2015]. The size of the intergranular facets ($\sim 150\text{-}200\mu\text{m}$) (Figure9b and c) confirms that the fatigue crack front is located in the coarse grain zone of the first layer HAZ. Mixed mode of large facets of intergranular fracture located at

the interface between fatigue crack front and brittle fracture area were generally observed for the specimens investigated.

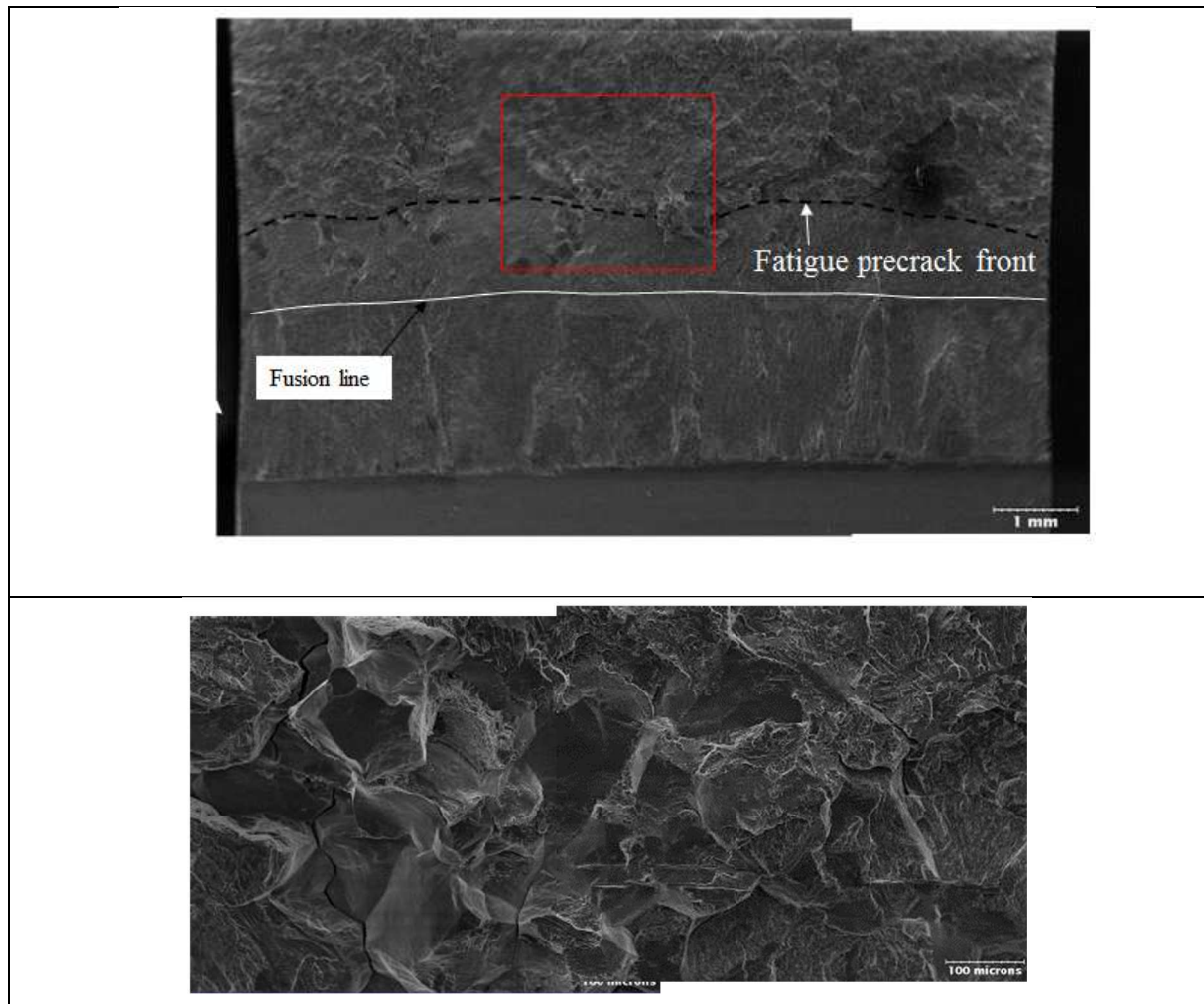


Figure 8: Fractographic investigations of CG_HAZ at unirradiated state. $KJc(1T) = 36.5 \text{ MPa}\cdot\text{m}^{0.5}$ à -115°C . Top: location of the initiation area on the fracture surface. Bottom: mixed mode of transgranular cleavage fracture and

intergranular fracture at the initiation site.

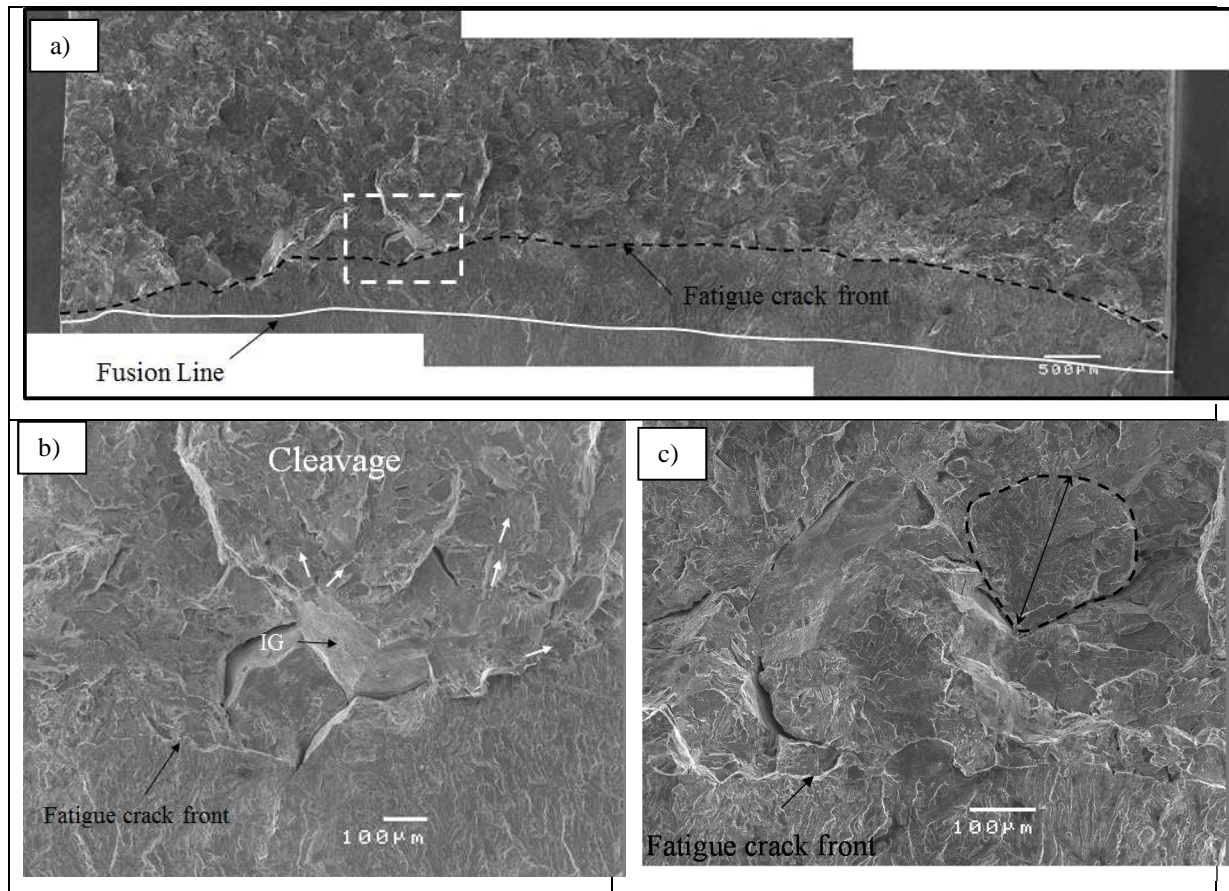


Figure 9: Fractographic investigations of CG-HAZ. Irradiated specimen : $KJc(1T) = 48.1 \text{ MPa}\cdot\text{m}^{0.5}$ à -20°C . a) location of the initiation area on the fracture surface. b) Intergranular facets (IG) at the initiation site. c) coarse facet indicated by dashed line.

Brittle fracture mode for FGHAZ is shown on Figure 10 for an irradiated specimen with a fracture toughness level of $54.8 \text{ MPa}\cdot\text{m}^{0.5}$ which correspond to the lowest value obtained at -50°C . The brittle mode corresponds to cleavage fracture. The finest cleavage facet size is shown on figure 10b and is consistent with a grain size of $\sim 10\mu\text{m}$ shown in Figure 1a. No modification of brittle fracture mode was observed

between un-irradiated and irradiated state for this level of fluence of $11.6 \cdot 10^{19} \text{ n.cm}^{-2}$.

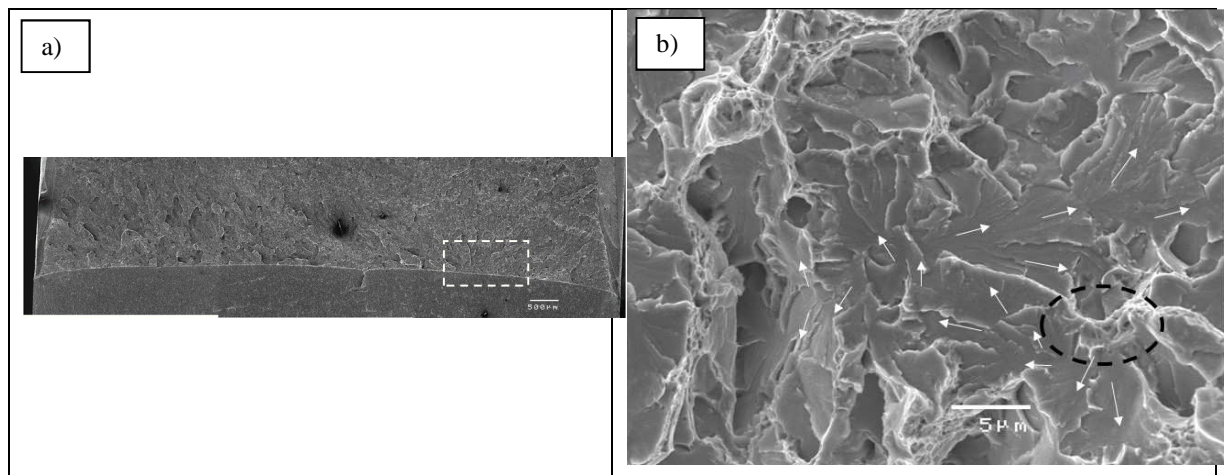


Figure 10: Fractographic investigations of FG-HAZ. Irradiated specimen: $KJc(1T) = 54.8 \text{ MPa.m}^{0.5}$ à -50°C . a) location of the initiation area on the fracture surface. b) Initiation site of cleavage fracture (indicated by a dashed line)

Conclusions

A R&D program was carried out by CEA, EDF and FRAMATOME to generate fracture toughness data to complement the irradiation surveillance program in a higher fluence range and including underclad heat affected zones. The irradiation exposure was performed in OSIRIS reactor at CEA Saclay up to maximum fluence level of $14 \cdot 10^{19} \text{ n/cm}^2$ ($E > 1\text{MeV}$). Fracture toughness properties were characterized for two base metals, a fine grain and a coarse grain HAZ and a weld metal base with PCCV specimens. The fracture toughness data were analyzed with the Master Curve methodology and compared to the RCC-M lower bound curve. The following conclusions can be drawn:

- A significant irradiation hardening is observed after irradiation for all the metallurgical zones considered.
- At a normalized fluence level of $12,4 \cdot 10^{19} \text{ n/cm}^2$ ($E > 1\text{MeV}$), fine grain HAZ has the highest fracture toughness (lowest T_0) and coarse grain HAZ shows a similar fracture toughness to that of the base metal ($T_0 = -7^\circ\text{C}$ and -6°C).
- The weld metal shows less scatter than BM and HAZ and appears to be well described by the master curve. This metallurgical zone has the highest T_0 in unirradiated and irradiated conditions.
- The lower bound character of the RCC-M curve is verified for all the cases.
- The RT_{NDT} of the base metal is shown to be appropriate for indexing the fracture toughness reference curve of underclad HAZ.
- Mixed intergranular and transgranular fractures are observed on CGHAZ but pure transgranular fracture is observed on FG HAZ specimens.

Acknowledgment

Support from LECI hot cells staff is greatly acknowledged. This program was supported by CEA-EDF-FRAMATOME R&D Institute I3P.

References

- [ASTME1921] ASTM E1921-08: Standard test method for determination of reference temperature T_0 for ferritic steels in the transition range.
- [Brillaud1992] C. Brillaud, F. Hedin, "In-Service Evaluation of French Pressurized Water Reactor Vessel Steel", Effects of Radiation on Materials : 15th International Symposium, ASTM STP 1125, R. E. Stoller, A. S. Kumar, and D. S. Gelles, Eds., American Society for Testing and Materials, Philadelphia, 1992, pp. 23-49.

- [Bouchet2005] C. Bouchet, B. Tanguy et al , "Benchmark on the determination of the cleavage triggering sites in a RPV steel in the DBT range",.11th International Conference on Fracture. Turin, March 20-25, 2005
- [Chapuliot2010] S. Chapuliot, D. Lauerova, M. Brumovsky,B. Tanguy, "Information about WPS experiments performed in NRI Rez and their evaluation", International symposium Fontevraud 7, Avignon, France, 26-30 September 2010
- [ISO12135] Norme ISO 12135. Matériaux métalliques – Méthode unifiée d'essai pour la détermination de la ténacité quasi-statique-Décembre 2002.
- [ISO6992] Norme ISO 6892-1-2-3. Matériaux métalliques – Essais de traction.
- [Joyce2001]J.A. Joyce and R.L. Tregoning, "Development of the T0 reference temperature from precracked Charpy specimens", Engineering Fracture Mechanics 68, 7, 2001, 861–894.
- [Joyce2005]J.A. Joyce and R.L. Tregoning, "Determination of constraint limits for cleavage initiated toughness data",Engineering Fracture Mechanics 72, 2005, 1559–1579.
- [Lucon2003] E. Lucon, M. Scibetta, E. Van Walle, « Assessment of the master curve approach on three reactor pressure vessel steels”n Intre. Journal of Fracture 119, 2003, 161-178.
- [Marini, 2015] B. Marini, X. Averty, P. Wident, P. Forget, F. Barcelo, Effect of the bainitic and martensitic microstructures on the hardening and embrittlement under neutron irradiation of a reactor pressure vessel steel, Journal of Nuclear Materials 465 (2015) 20-27
- [Tanguy2005] B. Tanguy, J. Besson, R. Piques, A. Pineau, Ductile to brittle transition of an A508 steel characterized by Charpy impact test. Part I: experimental results” Eng. Fract. Mech., 72, 2005, 49-72
- [Todeschini2010] P. Todeschini, Y. Lefevre, H. Churier-Bossennec, N. Rupa, G. Chas, C. Benhamou, "Revision of the irradiation embrittlement correlation used for the EDF RPV fleet", International symposium Fontevraud 7, Avignon, France, 26-30 September 2010
- [Todeschini2014] P. Todeschini, H. Churier-Bossennec, J-M Frund, J-P. Massoud," Effects of thermal ageing on toughness properties of pressure vessel steel" International symposium Fontevraud 8, Avignon, France 14-18 September 2014